LBL-34890
Preprint

Lawrence Berkeley Laboratory
UNIVERSITY OF CALIFORNIA

Materials Sciences Division

Submitted to Journal of the Electrochemical Society

Effect of Ion Implantation on the Corrosion Behavior of Lead and a Lead-Antimony Alloy

S.T. Zhang, F.P. Kong, and R.H. Muller

December 1993

Prepared for the U.S. Department of Energy under Contract Number DE-AC03-76SF00098

DISCLAIMER

LBL-34890

EFFECT OF ION IMPLANTATION ON THE CORROSION BEHAVIOR OF LEAD AND A LEAD-ANTIMONY ALLOY

S. T. Zhang, F. P. Kong, and R. H. Muller
Materials Sciences Division
Lawrence Berkeley Laboratory
University of California
Berkeley, CA. 94720

December 1993

This work was supported by the Assistant Secretary for Conservation and Renewable Energy, Office of Transportation Technologies, Electric and Hybrid Propulsion Division of the U.S. Department of Energy under Contract No. DE-AC03-76SF00098.

EFFECT OF ION IMPLANTATION ON THE CORROSION BEHAVIOR OF LEAD AND A LEAD-ANTIMONY ALLOY

S. T. Zhang*, F. P. Kong, and R. H. Muller
Materials Sciences Division
Lawrence Berkeley Laboratory
University of California
Berkeley, CA. 94720

Abstract

Ion implantation in Pb and Pb-4% Sb has been found to improve the open-circuit corrosion resistance of the two metals in 5M H_2SO_4. Titanium ions were implanted under different conditions of ion dose and ion energy. Optimum implantation conditions resulted in an up to 72-fold reduction of corrosion currents. The implantation of V, Cr, Ni, and W has been investigated for one implantation condition and has also resulted in decreased corrosion currents. The corrosion behavior was characterized by the current response to small anodic potential steps. Surface analysis and depth profiles have shown the importance of the spacial distribution of the implanted ions for their effects on the anodic and cathodic parts of the corrosion reactions.

* Present Address: Department of Applied Chemistry,
Chongqing University
Sichuan 630044, P.R. China

Introduction

Grid corrosion, particularly in the positive plate, is an important factor that limits the cycle life of lead-acid batteries. It has received considerable attention. Corrosion properties of positive grids have been improved by the use of alloys [1]. Antimony , in particular, has been shown to improve corrosion resistance, castability and strength [2], although accelerated corrosion caused by antimony at high anodic potentials has also been reported [3].

In the present work, the effect of surface modification by ion implantation on the corrosion of grid materials has been investigated. Titanium was used for implantation under different conditions of dosage and energy because of the corrosion resistance of this metal in sulfuric acid and its previous use as a substrate for lead dioxide [4]. Also, titanium implantation has been found to reduce the corrosion of iron [5]. The implantation of several other elements was also investigated for a single implantation condition. Pure lead (99.99%) and a lead-4% antimony alloy were chosen as representative grid materials.

Ion implantation is used extensively for the doping of semiconductors in integrated circuit technology [6] but it is a relatively new technique to alter the surface properties of metals. The process makes it possible to generate metastable solid solutions of the implanted element in the host material that cannot be obtained by conventional metallurgical alloying techniques [7, 8]. The composition of the implanted layers can be controlled by the implantation *dose*, their location with respect to the surface by the implantation *energy*.

The technique has been used to modify surface properties of metals such as hardness and corrosion resistance [8, 9], friction and wear resistance [9, 10, 11]. For example, ion implantations with tantalum, lead, and argon into iron have resulted in improved corrosion resistance [7, 12, 13]; implantation of tantalum into aluminum has increased the pitting potential in chloride solution [14], and the implantation of tantalum and chromium into M50 steel has shifted the passive breakdown potential to more positive values [15]. The reasons for the observed effects, however, have not received much attention, although dislocations have been found to extend much deeper below the surface than the implanted ions [16] and surface roughening by argon implantation into iron has resulted in an increased thickness of the air-formed film [13]. The application of a barium metablumbate coating by thermal processing has been reported to improve the corrosion resistance of lead/acid battery grid materials [17], but ion implantation does not seem to have been used for this purpose so far.

Experimental procedures

The ion implantations were performed with a new high-current, pulsed ion beam that employs a metal vapor vacuum arc source and has been described elsewhere [18, 19]. The purity of the ion source cathode materials was 99.99%. Typical beam current densities were 2.55 mA/cm^2, typical pulse durations 0.24 ms, and pulse frequencies 5-10 Hz. The extraction voltage (which together with the ionic charge determines the beam energy) was 30-100 kV, and implantation doses of $1x10^{15}$ to $5x10^{17}$ atoms/cm^2 were used.

Corrosion rates of the grid materials were derived from the current response of the specimens in 5M H_2SO_4 to small anodic potential steps (3-10 mV vs. open circuit, $Pb/PbSO_4$, potential), extrapolated from short-term measurements to zero time (in order to represent the behavior of the original surface and avoid concentration polarization). This first step in the corrosion measurement is illustrated in Fig. 1 for an applied potential of 8 mV. The corrosion current density i_{corr} was derived from the slope of the zero - time current density $i_{t=0}$ plotted vs. the applied potential η, illustrated in Fig.2, according to eq. (1),

$$i_{t=0} = i_{corr}\, nF\eta/RT \qquad (1)$$

where n is the valence of the corrosion product (n=2 for $PbSO_4$), F is the Faraday constant (F=96487 Coul/mole), R is the Ideal Gas Constant (R=8.314 J/deg mole), and T is the absolute temperature (T=298K). Although this simple approach does not attempt to consider the formation of dissolved reaction products [20] in addition to the solid phase nor the double layer charging currents, it provides a valid comparison between samples before and after ion implantation.

The potential steps were generated by a PAR 273 Potentiostat/Galvanostat, controlled by an IBM 50 computer. The working electrodes were prepared from pure lead (99.99%) and lead-4% antimony alloy in the Materials Fabrication Facility of the Laboratory. The reference electrode was $Hg/HgSO_4$ in the same electrolyte as in the cell and all potentials reported are relative to

this reference. The counter electrode was a large (8 cm^2) lead sheet. Constant current experiments were performed with the same system. The electrolyte used in all experiments was 5M H_2SO_4 , prepared from analytical sulfuric acid and distilled water. All measurements were conducted at room temperature.

Surface morphology and composition were determined by scanning electron microscopy (SEM, International Scientific Instruments WB-6) and energy dispersive x-ray spetroscopy (EDS, Ortec 5000). Depth profiles of implanted Ti were determined by Auger electron spectroscopy (AES) and argon ion bombardment (Physical Electronics PHI 660 Scanning Auger Microscope). Before implantation, specimen surfaces for later SEM and AES were smoothed by pressing against polished stainless steel at 69-103 MPa (10000 -15000 psi), which resulted in a mirror-like surface finish. Specimens for current measurements were mounted in epoxy resin, exposing a 1.4x1.4 cm working area which was polished with diamond paste to 1 μm.

Results and Discussion

Corrosion current density. Corrosion current densities, determined according to eq.1, are shown in Fig.3 for pure Pb and Pb-4% Sb substrates as a function of the *dose* of Ti ions implanted at a fixed ion energy of 60 keV. These corrosion current densities compare to 5.4 mA/cm^2 for Pb and 2.9 mA/cm^2 for Pb-4%Sb before implantation, shown at zero dose. It can be seen that for both substrates the corrosion currents are greatly lowered by the ion implantation, with a minimum being reached for Pb at a dose of $5x10^{16}$ ions

/cm^2. The effect of Ti ion *energy* at a fixed dose of $5x10^{16}$ ions/cm^2 is illustrated in Fig. 4, which shows a shallow minimum in corrosion current density near 60 keV for both substrates. An optimum dose has also been reported for wear resistance and friction coefficient with nitrogen implantation into titanium [21].

Surface analysis. Some reasons for the observed minima of corrosion currents as functions of ion dose and energy can be gleaned from the spacial distribution of the implanted Ti. Fig.5 shows measured depth profiles of Ti in the two substrate materials for different implantation energies. It can be seen that for the optimum energy of 60 keV the peak of the Ti concentration lies at about 40 and 60 nm, resp., under the surface (projected range) and Ti can be found to a depth of about 100 nm (longitudinal straggling), which is comparable to the extent of the corrosion reaction; also, the Ti content at the surface is appreciable. At the lower implantation energy, the implanted material is located so close to the surface (peak at 25 and 30 nm, resp.) that it can be removed by corrosion. Surface concentration of Ti may also be excessive. At the higher implantation energies the implanted material is buried too deep and its concentration at the surface is too small to affect corrosion reactions.

Further evidence on the action of Ti is obtained by the surface analysis of the implanted specimens with SEM and EDS before the corrosion measurements. After low-dose implantation, Ti is found to be uniformly distributed on the surface, as would be expected for a solid solution. After high-dose implantation, however, a segregation of Ti occurs, which could be seen as

light areas in SEM surface images and were identified as Ti-rich regions by EDS. Fewer Ti-rich particles were observed on the antimony alloy than on the pure lead, which qualitatively agrees with the smaller effect of high implantation dose on corrosion current, shown in Fig. 3. For Ti doses of $5x10^{16}$ and $1x10^{17}$ atoms/cm^2 in the antimony alloy, the local concentration of Ti was independent of the locally varying Sb concentration, indicative of a uniform Ti distribution (Fig. 6), while for the higher dose of $5x10^{17}$ atoms/cm^2 an accumulation of Ti in Sb-rich regions of the alloy is associated with Ti segregation, which can lead to the formation of microcells and the catalysis of H_2 evolution. Ti distribution was independent of implantation pulse frequency.

Anodic and cathodic reactions. Some mechanistic insight into the action of titanium implantation can also be gleaned from time-dependent potential measurements under constant current. The effect of the implantation *dose*, for a fixed energy of 60 keV, on anodic and cathodic behavior is shown in Figs. 7 and 8. The charge passed at the potential plateau of -1.04 V is decreased by the implantation. This plateau corresponds to the formation of $PbSO_4$ until the onset of passivation [22, 23] and the formation of PbO and PbO_2 or Sb_2O_3 [24, 25]. The anodic part of the corrosion reaction is therefore greatly inhibited by Ti implantation, with an implantation dose higher than the optimum of $5x10^{16}$ atoms/cm^2 producing slightly less favorable results. Similar cathodic transients, obtained after fixed anodic polarization (26 min at 0.26 mA/cm^2), show steps in potential for the reduction of different oxides and sulfates [24, 26, 27, 28, 29, 30] and terminate with hydrogen evolution as the last step. Ion implantation reduced the overpotential for hydrogen evolution. This acceleration of the cathodic part of the corrosion reaction

indicates a catalytic effect of Ti. The reduction in overpotential is larger for the pure lead substrate than for the lead-antimony alloy and it increases for both materials with increasing implantation dose, as shown in Fig. 8. The reduction in overpotential is particularly marked for the lead substrate once the optimum dose is exceeded and Ti segregation on the surface occurs. In agreement with the literature [31], the hydrogen overpotential on the Pb-Sb alloy is lower than on pure Pb. An optimum dose of 5.5×10^{16} atoms/cm^2, which resulted in a large reduction in the corrosion of Fe, has been reported for the implantation of Pb at 400 keV; it was associated with a reduced cathodic current density [32].

The effect of the *energy* of the implanted Ti ions on electrochemical behavior is shown in Figs. 9 and 10 for a fixed dose of 5×10^{16} atoms /cm^2. It can be seen from the anodic polarization, Fig. 9, that for both substrates implantation energies below and above the optimum of 60 keV result in larger amounts of lead sulfate corrosion product. The cathodic polarization exhibits a lowering of the hydrogen evolution overpotential with decreasing Ti ion energy, shown in Fig. 10 together with the overpotentials before implantation. It can be seen that the deep implantation at 90 keV into pure Pb has almost no effect on H_2 evolution.

Other elements. Corrosion current measurements after the implantation of V, Cr, Ni, and W into Pb and Pb-Sb under one implantation condition each are given in table 1, which also includes the results with Ti for comparison. It can be seen that all of these surface treatments have resulted in decreased corrosion current densities. Optimization of some of these treatments may

well produce effects comparable to those obtained with Ti.

Conclusions

1. Ion implantation of several elements into Pb and Pb-4% Sb has been shown to decrease the open-circuit corrosion current density in 5M H_2SO_4. For the implantation of Ti, an optimum dose of $5x10^{16}$ atoms/cm^2 at an optimum energy of 60 keV have resulted in a 36 and 72-fold decrease for the two substrate materials, respectively.
2. Insufficient protection was obtained with very low implantation *dose*, where a protective layer could not be formed and with very large dose, where Ti segregation on the surface occurred. Very low implantation *energy* resulted in a protective layer that was too thin, in addition to being prone to Ti segregation on the surface. Very large implantation energy resulted in Ti implantation to be too deep to affect reactions at the electrode surface.
3. Anodic and cathodic parts of the corrosion reaction are affected in opposite ways by Ti implantation, which accounts for minima in the corrosion current as functions of implantation energy and dose. While the anodic reaction ($PbSO_4$ formation) is inhibited by the implantation, the cathodic reaction (H_2 evolution) is accelerated, particularly for high Ti concentrations or Ti segregation at the surface, resulting from low implantation energy or high dose. As a result, control of the rate of corrosion changes at the minima from the anodic to the cathodic reaction.

4. Limited observations with the implantation of other elements showed various degrees of decreases in corrosion currents. Some of these are close enough to the observations with Ti implantation that a search for optimized implantation conditions may be worthwhile.

Acknowledgments

We thank I. G. Brown of the Lawrence Berkeley Laboratory for his help and the use of his ion implantation equipment.

This work was supported by the Assistant Secretary for Conservation and Renewable Energy, Office of Transportation Technologies, Electric and Hybrid Propulsion Division of the U.S. Department of Energy under Contract No. DE-AC03-76SF00098.

This paper was presented at the Toronto meeting of the Society, Oct. 11-16, 1992, extended abstract No. 60.

References

[1] D. E. Swets, J. Electrochem. Soc., **120**, 925 (1973).

[2] S. Webster, P. J. Mitchell, N. A. Hampson, and J. I. Dyson, J. Electrochem. Soc., **133**, 133 (1986).

[3] J. L. Weininger and E. G. Siwek, J. Electrochem. Soc., **123**, 602

[4] J. Feng and D. C. Johnson, J. Electrochem. Soc., **138**, 3328 (1991).

[5] Y. Okabe, M. Iwaki. K. Takahashi, and K. Yoshida, Jap. J. Appl. Phys., **22**, L165 (1983).

[6] T. C. Smith, Nucl. Instrum. Methods Phys. Res., **B21**, 90 (1987).

[7] V. Ashworth, D. Baxter, W. A. Grant, and R. P. M. Procter, Corros. Sci., **17**, 947 (1977).

[8] V. Ashworth, D. Baxter, W. A. Grant, and R. P. M. Procter, Corros. Sci., **16**, 661 (1976).

[9] J. E. Barry, E. J. Tobin, and P. Sioshansi, Surface Coating Technol., **51**, 176 (1992).

[10] R. Wei, P. J. Wilbur, W.S. Sampath, D. L. Williamson, and L. Wang, J. Tribology, **113**, 166 (1991).

[11] J. Chen, J. Blanchard, J. R. Conrad, and R. A. Dodd, Surf. Coatings Technol., **53**, 267 (1992).

[12] V. Ashworth, W. A. Grant, R. P. M. Procter, and E. J. Wright, Corros. Sci., **18**, 681 (1978).

[13] V. Ashworth, W. A. Grant, and R. P. M. Procter, Corros. Sci., **16**, 393 (1976).

[14] P. M. Natishan, E. McCafferty, and G. K. Hubler, Nucl. Instrum. Methods Phys. Res., **B59/60**, 841 (1991).

[15] B. R. Nielsen, B. Torp, C. M. Rangel, M. H. Simplicio, A. C.

Consiglieri, M. F. DaSilva, F. Paszti, J. C. Soares, A. Dodd, J. Kinder, M. Pitaval, P. Thevenard, and R. G. Wing, Nucl. Instrum. Methods Phys. Res., **B59/60**, 772 (1991).

[16] A. N. Didenko, A. E. Ligachov, I. B. Kurakin, M. G. Sipailo, E. V. Kozlov, and J. B. Sharkeev, Surface Coating Technol., **51**, 186 (1992).

[17] W.-H. Kao, S. L. Haberichter, and K. R. Bullock, J. Electrochem. Soc., **139**, L105 (1992).

[18] I. G. Brown, M. R. Dickinson, J. E. Galvin, X. Godechot, and R A MacGill, J. Matls. Eng., **13**, 217 (1991).

[19] I. G. Brown, M. R. Dickinson, J. E. Galvin, X. Godechot, and R A MacGill, Nucl. Instrum. Methods Phys. Res., **B55**, 506 (1991).

[20] V. Danel and V. Plichon, Electrochim. Acta, **28**, 785 (1983).

[21] A. Mucha, and M. Braun, Surf. Coatings Technol., **50**, 135 (1992).

[22] L. M. Baugh and K. L. Bladen, J. Electroanal. Chem., **145**, 355 (1983).

[23] S. B. Hall and G. A. Wright, Corros. Sci., **31**, 709 (1990).

[24] M. N. C. Ijomah, J Electrochem. Soc., **134**, 2960 (1987).

[25] V. Danel and V. Plichon, Electrochim. Acta, **28**, 781 (1983).

[26] Y. Guo, J. Electrochem. Soc., **138**, 1222 (1991).

[27] F. E. Varela, L. M. Gassa, and J. R. Vilche, Electrochim. Acta, **37**, 1119 (1992).

[28] K. Kanamura and Z.-I. Takehara, J. Electrochem. Soc., **139**, 345 (1992).

[29] F. E. Varela, L. M. Gassa, and J. R. Vilche, Electrochim. Acta, **37**, 1119 (1992).

[30] C. Wei and K. Rajeshwar, J. Electrochem. Soc. **140**, L128 (1993).

[31] B. K. Mahato, J. L. Strebe, D. F. Wilkinson, and K. R. Bullock, J. Electrochem. Soc., **132**, 19 (1985).

[32] H. Ferber, H. Kasten, G. K. Wolf, W. J. Lorenz, H. Schweickert, and

H. Folger, Corros. Sci., 20, 117 (1980).

Figure Captions

Fig. 1 Determination of zero-time anodic current densities by extrapolation to zero time after application of a small anodic polarization, shown for 8 mV vs. open circuit potential. Pure Pb and Pb-4% Sb alloy specimens in 5M H_2SO_4. (a) Before ion implantation: extrapolated zero-time current densities 3.01 and 1.26 mA/cm^2 for Pb and Pb-Sb, respectively. (b) After ion implantation: 0.094 and 0.024 mA/cm^2 resp..Conditions for Ti ion implantation: ion dose $5x10^{16}$ atoms/cm^2, ion energy 60 keV, ion pulse peak current density 2.55 mA/cm^2, pulse duration 0.24 ms, pulse frequency 5 Hz.

Fig. 2 Zero-time current density as a function of applied potential for the determination of corrosion current densities i_{corr} from the slope of the plots by use of Eq.(1). Pure Pb and Pb-4% Sb alloy specimens in 5M H_2SO_4. (a) Before ion implantation: i_{corr} = 5.4 and 2.9 mA/cm^2 for Pb and Pb-Sb, respectively. (b) After ion implantation: i_{corr} = 0.15 and 0.04 mA/cm^2, resp.. Implantation conditions as in Fig. 1.

Fig. 3 Dependence of corrosion current density on *dose* of implanted Ti ions for pure Pb and Pb-4%Sb alloy. Ion energy 60 keV, other implantation conditions as in Fig. 1.

Fig. 4 Dependence of corrosion current density on *energy* of implanted

Ti ions for pure Pb and Pb-4%Sb alloy. Ion dose $5x10^{16}$ atoms/cm^2, other implantation conditions as in Fig. 1.

Fig. 5 Depth profiles of Ti in pure Pb (a) and Pb-4%Sb alloy (b), after Ti implantation at different ion energies, with ion dose $5x10^{16}$ atoms/cm^2. Profiles measured by Auger electron spectroscopy and argon ion bombardment

Fig. 6 Correlation of local Ti and Sb surface concentrations, determined by EDS, in Pb-Sb alloy after Ti ion implantation under different conditions of dose and frequency. Implantation energy 60 keV

Fig. 7 Effect of implantation *dose* of Ti ions into Pb and Pb-Sb on $PbSO_4$ formation under constant anodic current (0.26 mA/cm^2). Charge passed (at -1.04V) to the potential rise associated with passivation and formation of oxides of Pb and Sb. Implantation ion energy 60 keV.

Fig. 8 Effect of implantation *dose* of Ti ions into Pb and Pb-Sb on hydrogen overpotential under constant cathodic current (-0.26 mA/cm^2). Implantation ion energy 60 keV.

Fig. 9 Effect of implantation *energy* of Ti ions into Pb and Pb-Sb on $PbSO_4$ formation under constant anodic current (0.26 mA/cm^2).

Charge passed at -1.04 V. Implantation ion dose $5x10^{16}$ atoms/ cm^2.

Fig. 10 Effect of implantation *energy* of Ti ions into Pb and Pb-Sb on hydrogen overpotential under constant cathodic current (-0.26 mA/cm^2). Implantation ion dose $5x10^{16}$ atoms/cm^2. Values before implantation shown at 100 keV.

Table 1 Effect of the ion implantation of different elements on the corrosion current density of lead and lead-4% antimony alloy in 5M sulfuric acid.

Implantation conditions						**Corrosion Current** (mA/cm^2)	
Element	**Energy** (keV)	**Dose** ($atoms/cm^2$)	**Peak current density** (mA/cm^2)	**Pulse duration** (ms)	**Pulse frequency** (Hz)	**Substrate**	
						Pb	**Pb-4%Sb**
Ti	60	$5x10^{16}$	2.55	0.24	5	0.15	0.040
V	60	$5x10^{16}$	2.55	0.24	10	0.20	0.053
Cr	60	$5x10^{16}$	2.55	0.24	10	0.27	0.093
Ni	60	$5x10^{16}$	2.55	0.24	10	0.18	0.085
W	180	$5x10^{16}$	2.55	0.24	~3	0.81	0.510
None	---	0	---	---	---	5.40	2.90

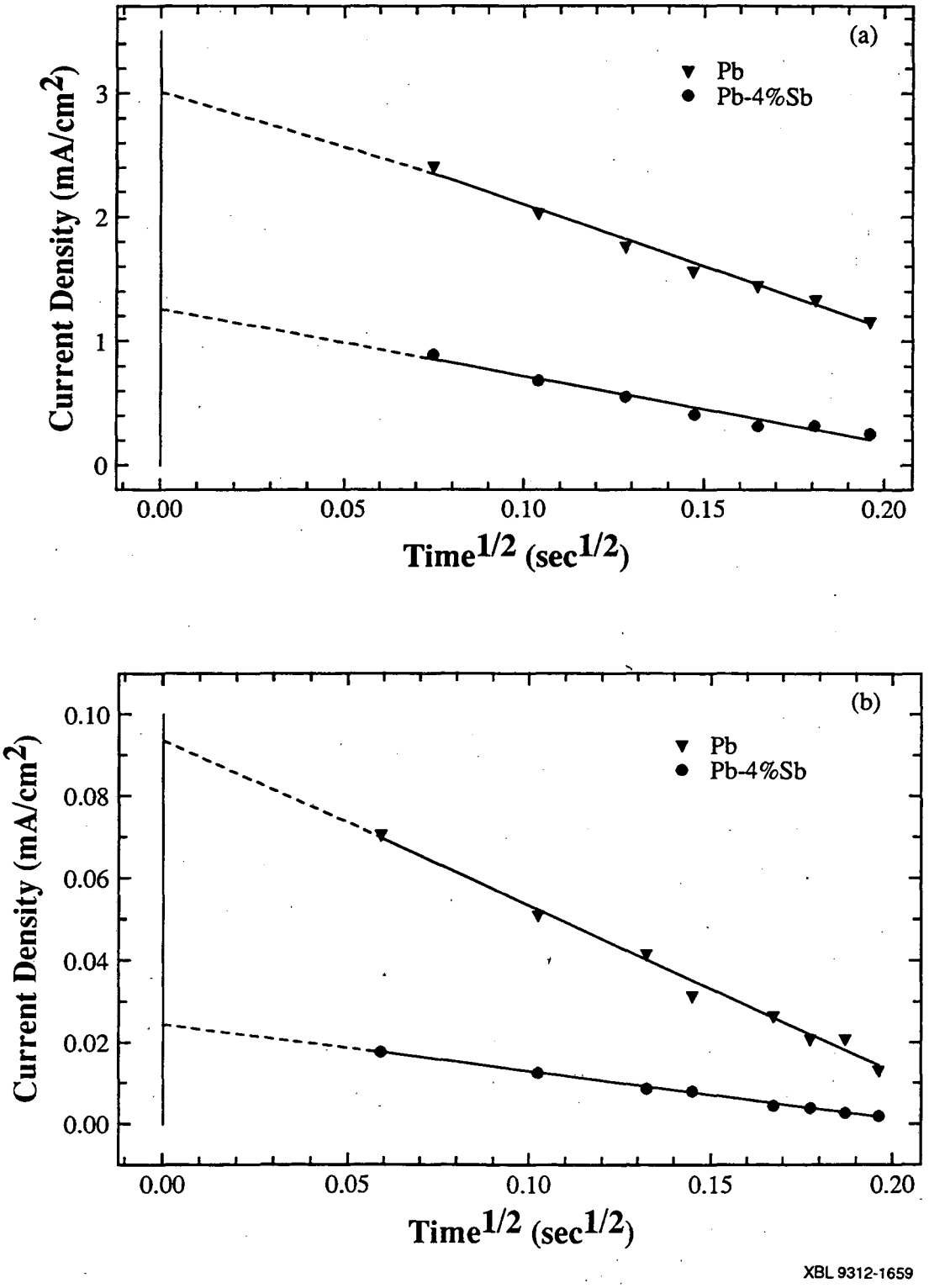
(a)
Pb
Pb-4%Sb
Current Density (mA/cm^2)
0
1
2
3
0.00
0.05
0.10
0.15
0.20
Time$^{1/2}$ (sec$^{1/2}$)
(b)
Pb
Pb-4%Sb
Current Density (mA/cm^2)
0.00
0.02
0.04
0.06
0.08
0.10
0.00
0.05
0.10
0.15
0.20
Time$^{1/2}$ (sec$^{1/2}$)
XBL 9312-1659

Fig. 1

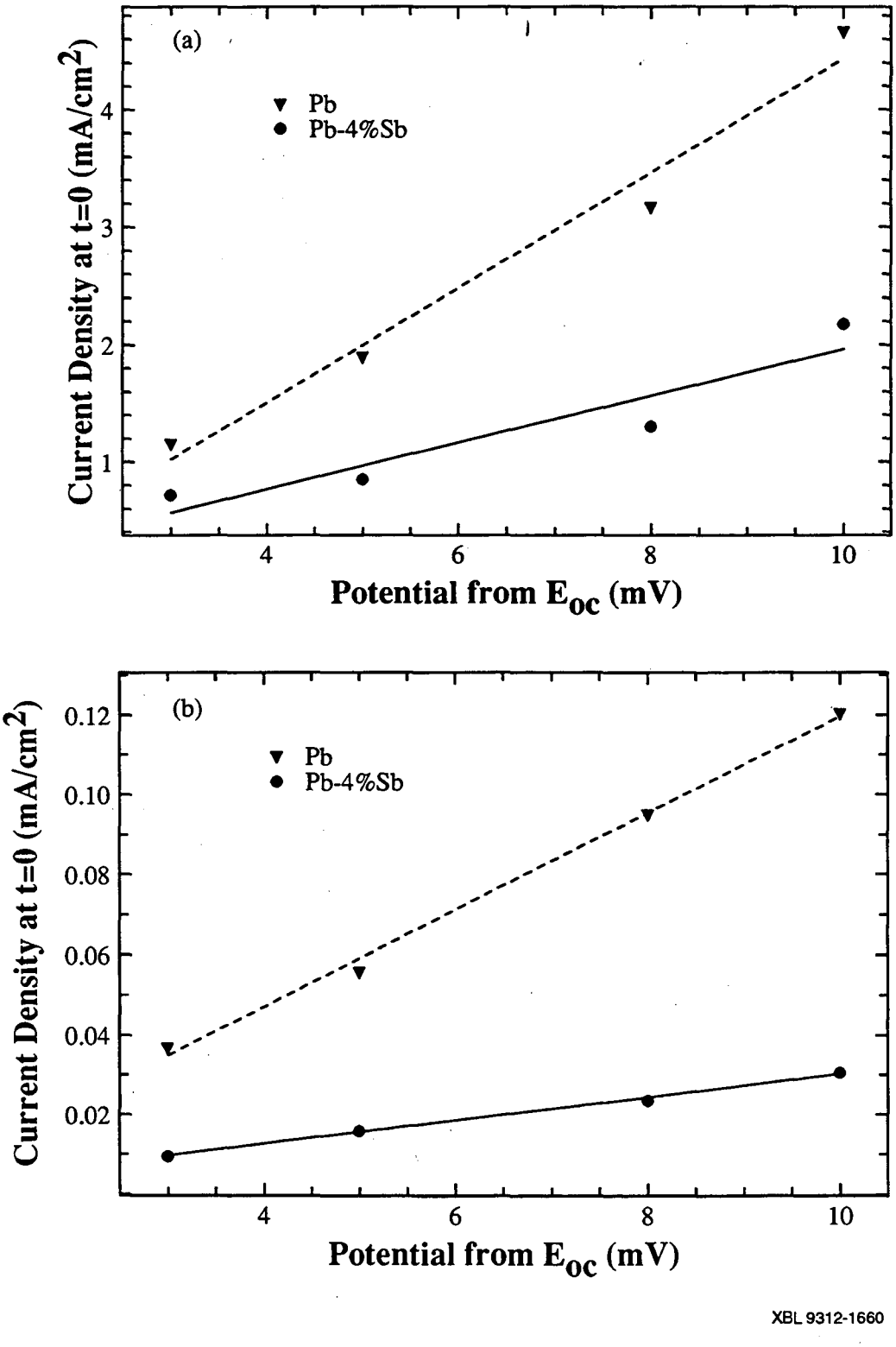
(a)
Pb
Pb-4%Sb
Current Density at t=0 (mA/cm2)
Potential from Eoc (mV)
(b)
Pb
Pb-4%Sb
Current Density at t=0 (mA/cm2)
Potential from Eoc (mV)
XBL 9312-1660

Fig. 2

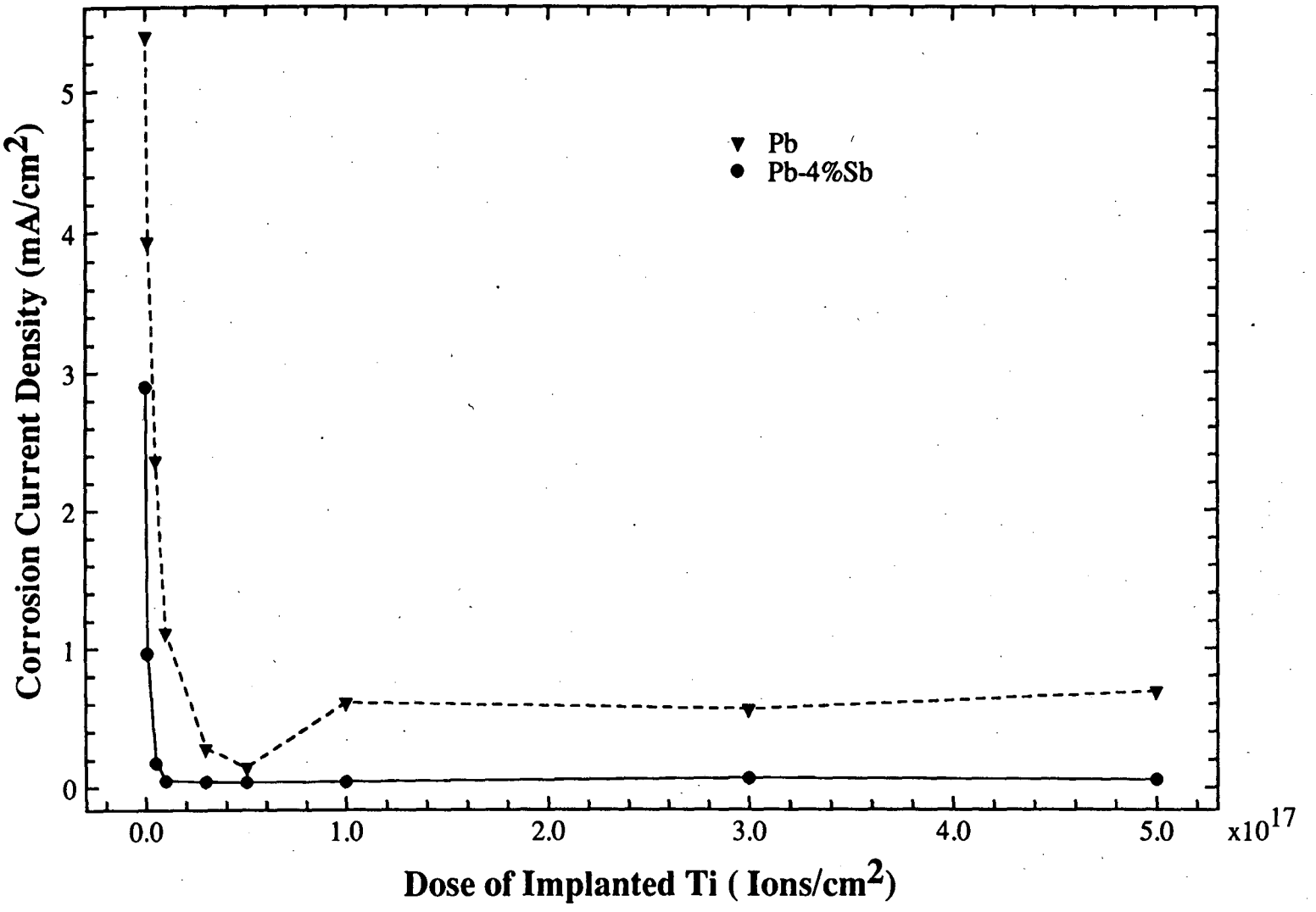
Corrosion Current Density (mA/cm2)
Dose of Implanted Ti (Ions/cm2)
Pb
Pb-4%Sb
0
1
2
3
4
5
0.0
1.0
2.0
3.0
4.0
5.0
x10^17
XBL 9312-1661

Fig. 3

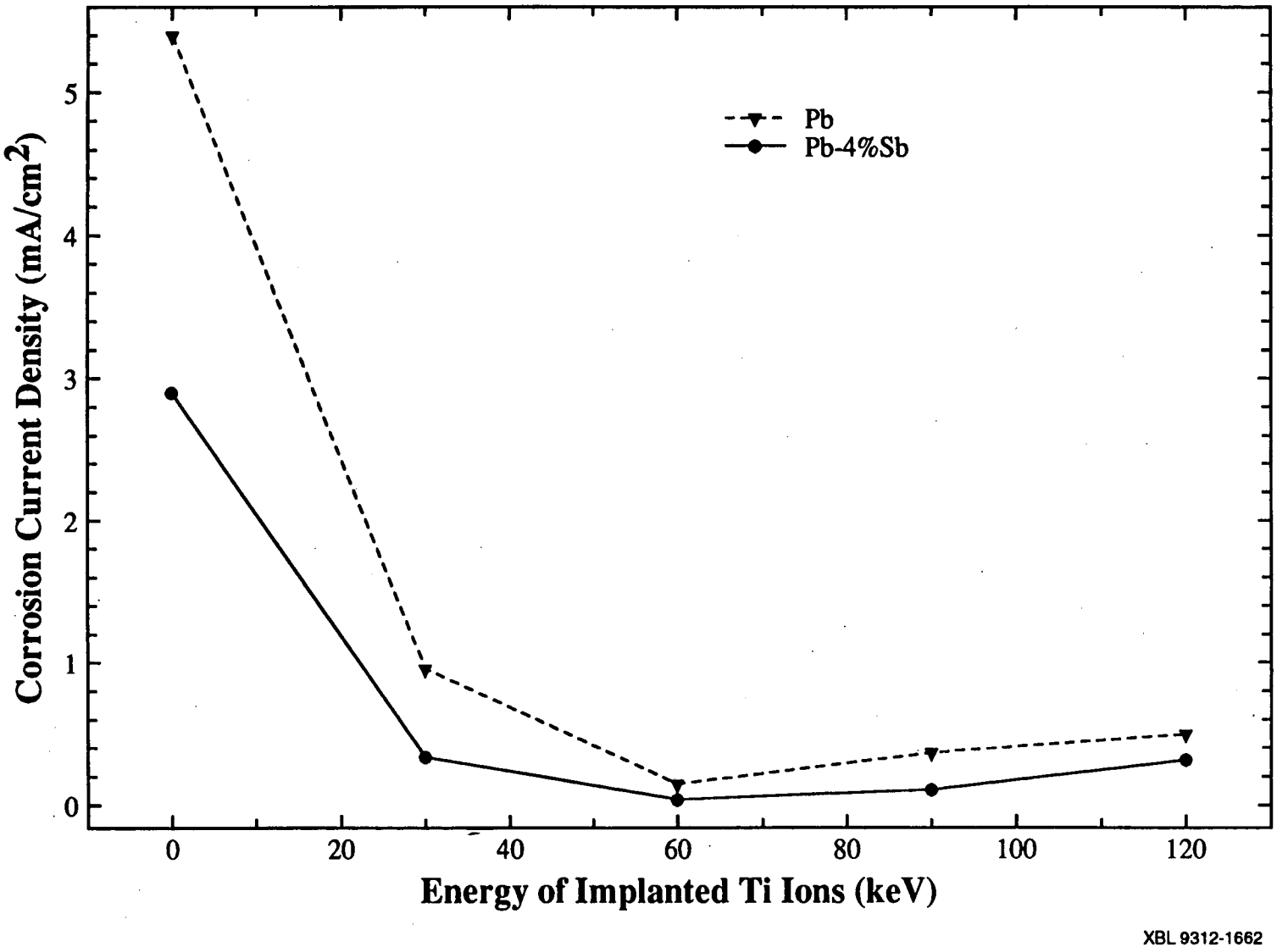
Corrosion Current Density (mA/cm^2)
Energy of Implanted Ti Ions (keV)
Pb
Pb-4%Sb
0
1
2
3
4
5
0
20
40
60
80
100
120
XBL 9312-1662

Fig. 4

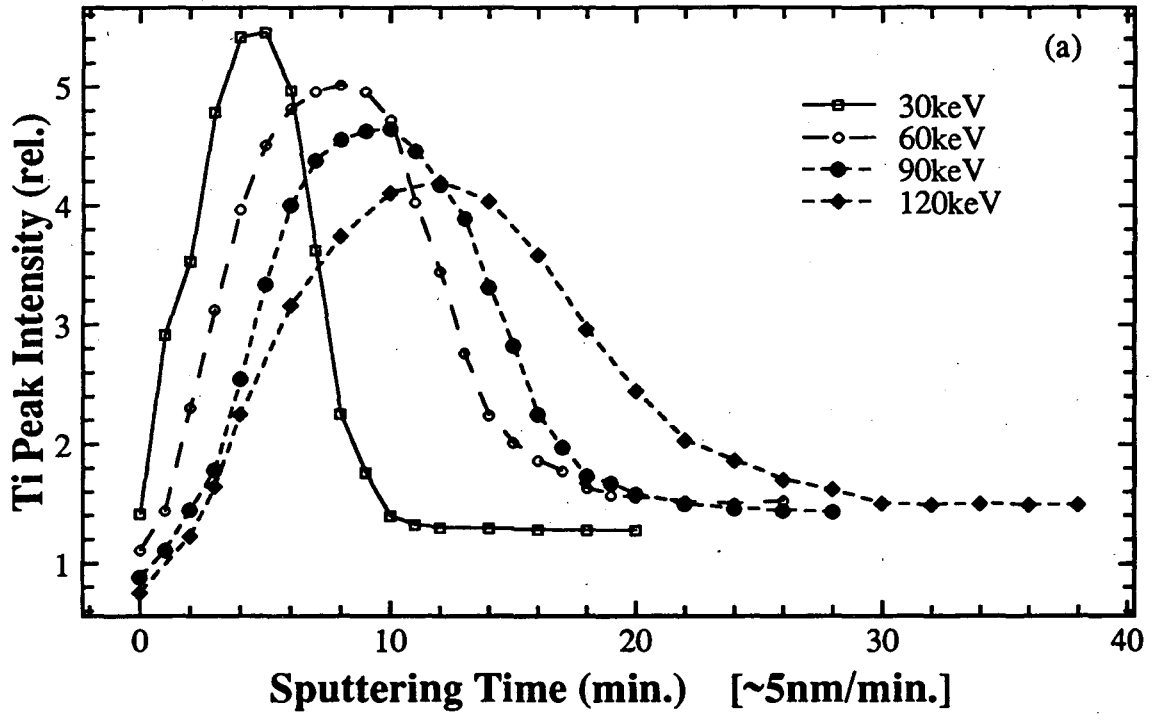

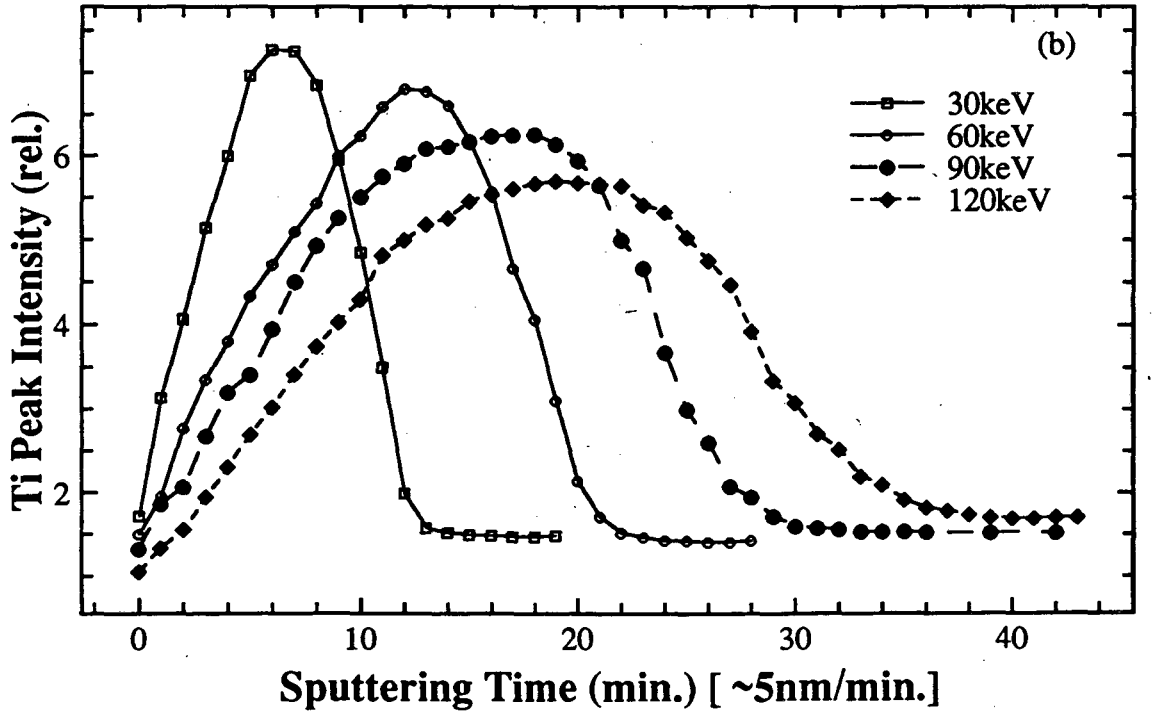

XBL 9312-1663

Fig. 5

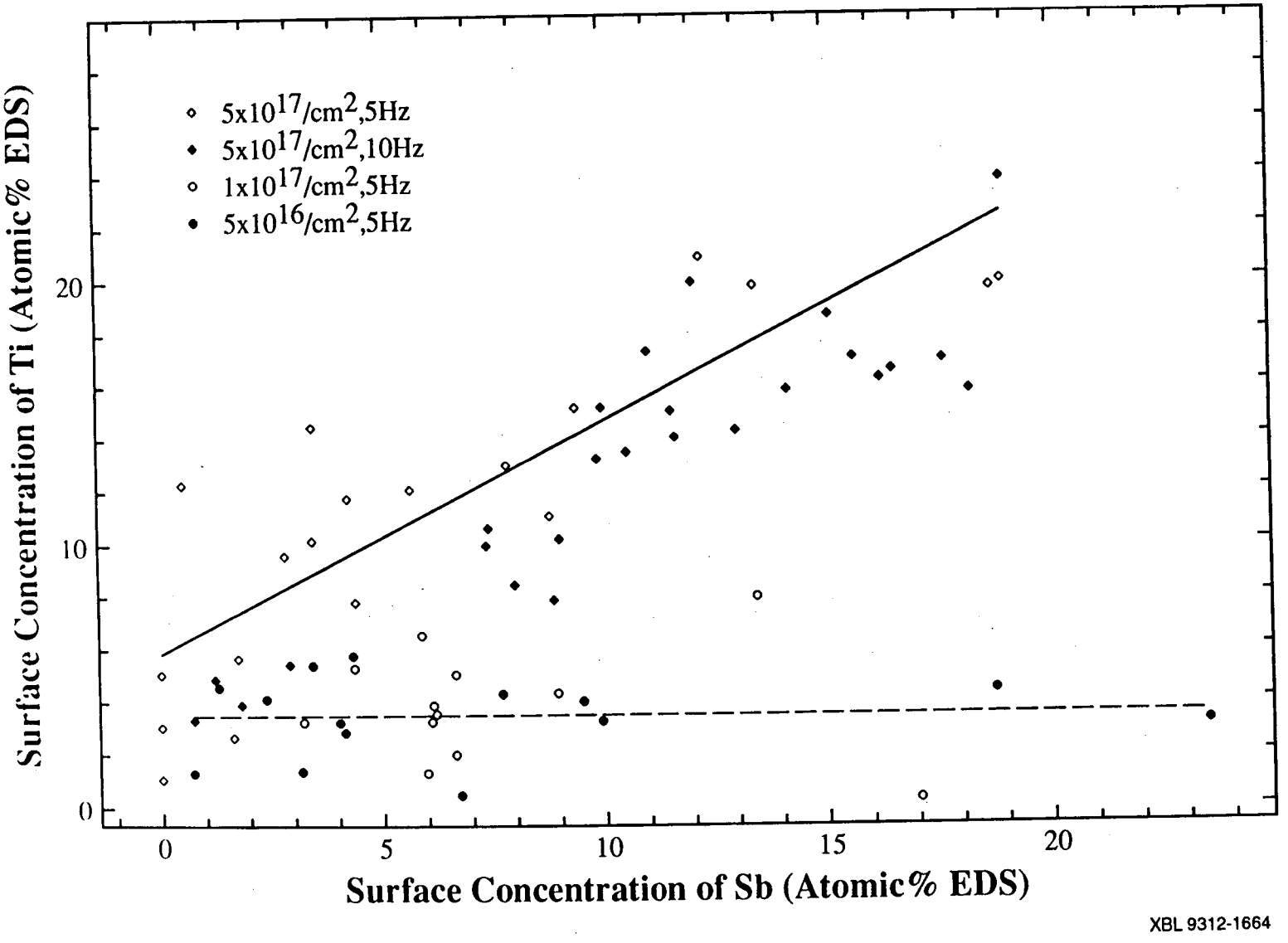
5x10^17/cm^2,5Hz
5x10^17/cm^2,10Hz
1x10^17/cm^2,5Hz
5x10^16/cm^2,5Hz
Surface Concentration of Ti (Atomic% EDS)
Surface Concentration of Sb (Atomic% EDS)
0
10
20
0
5
10
15
20
XBL 9312-1664

Fig. 6

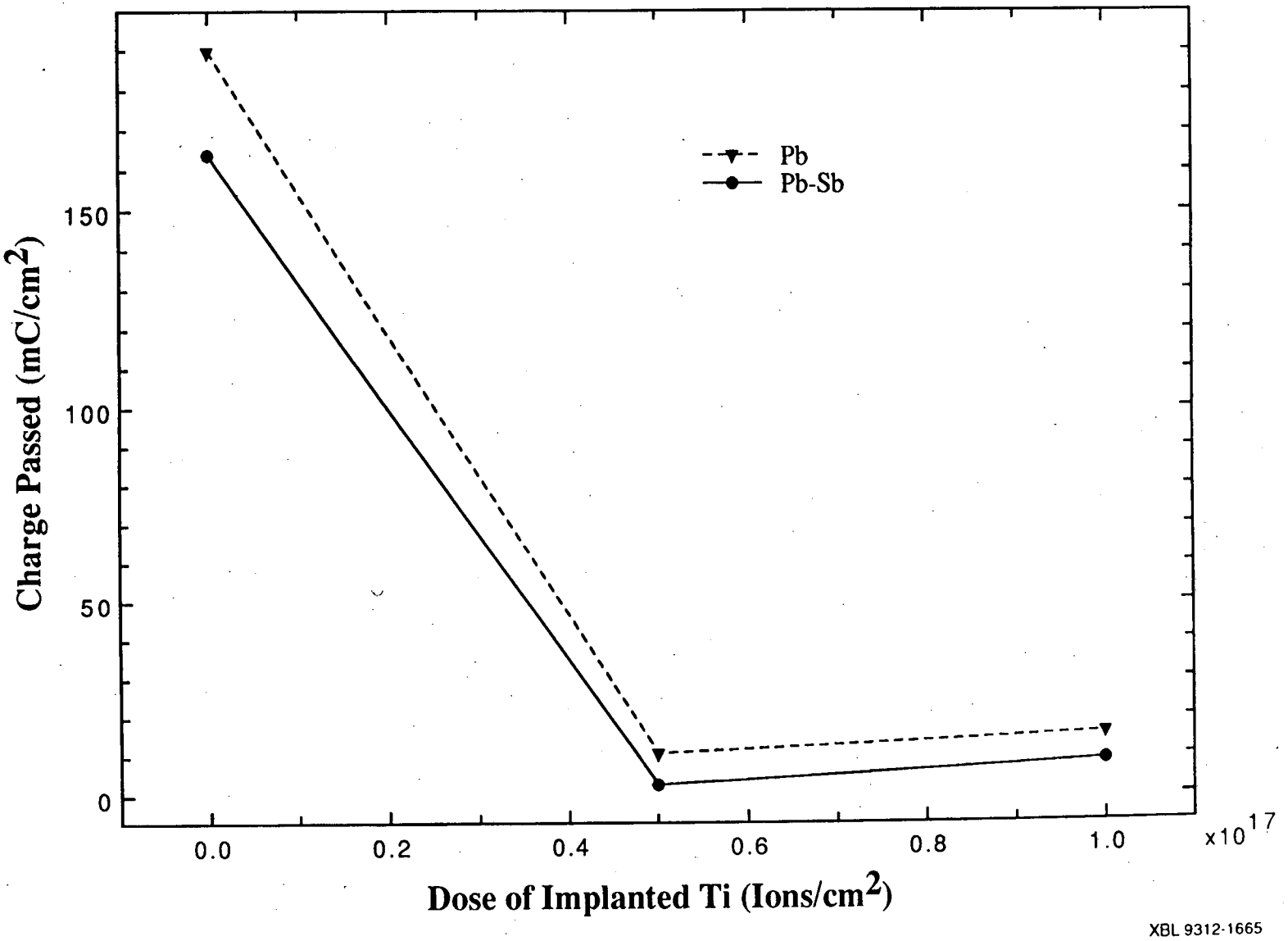
Pb
Pb-Sb
Charge Passed (mC/cm2)
150
100
50
0
0.0
0.2
0.4
0.6
0.8
1.0
x10 17
Dose of Implanted Ti (Ions/cm2)
XBL 9312-1665

Fig. 7

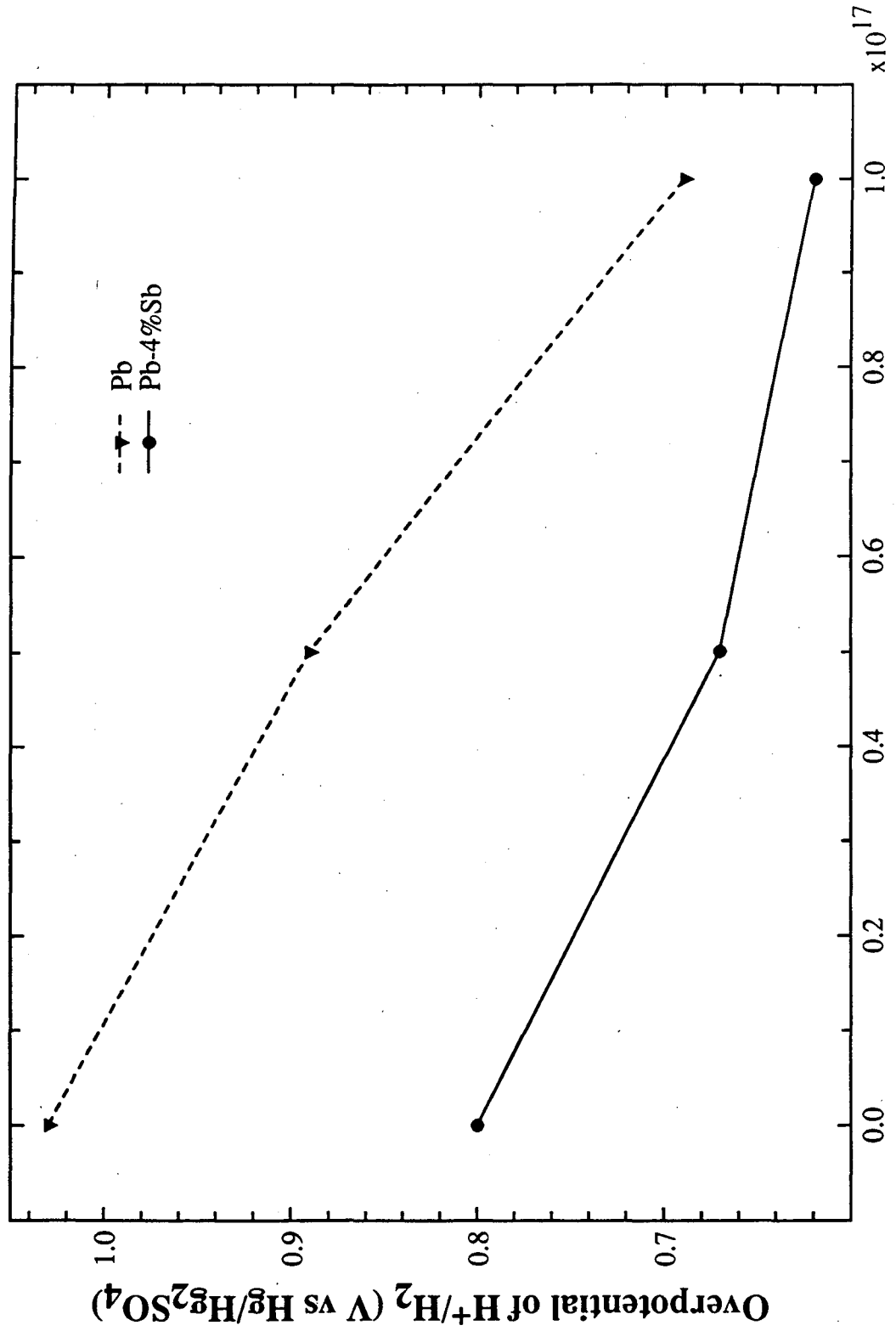

XBL 9312-1666

Fig. 8

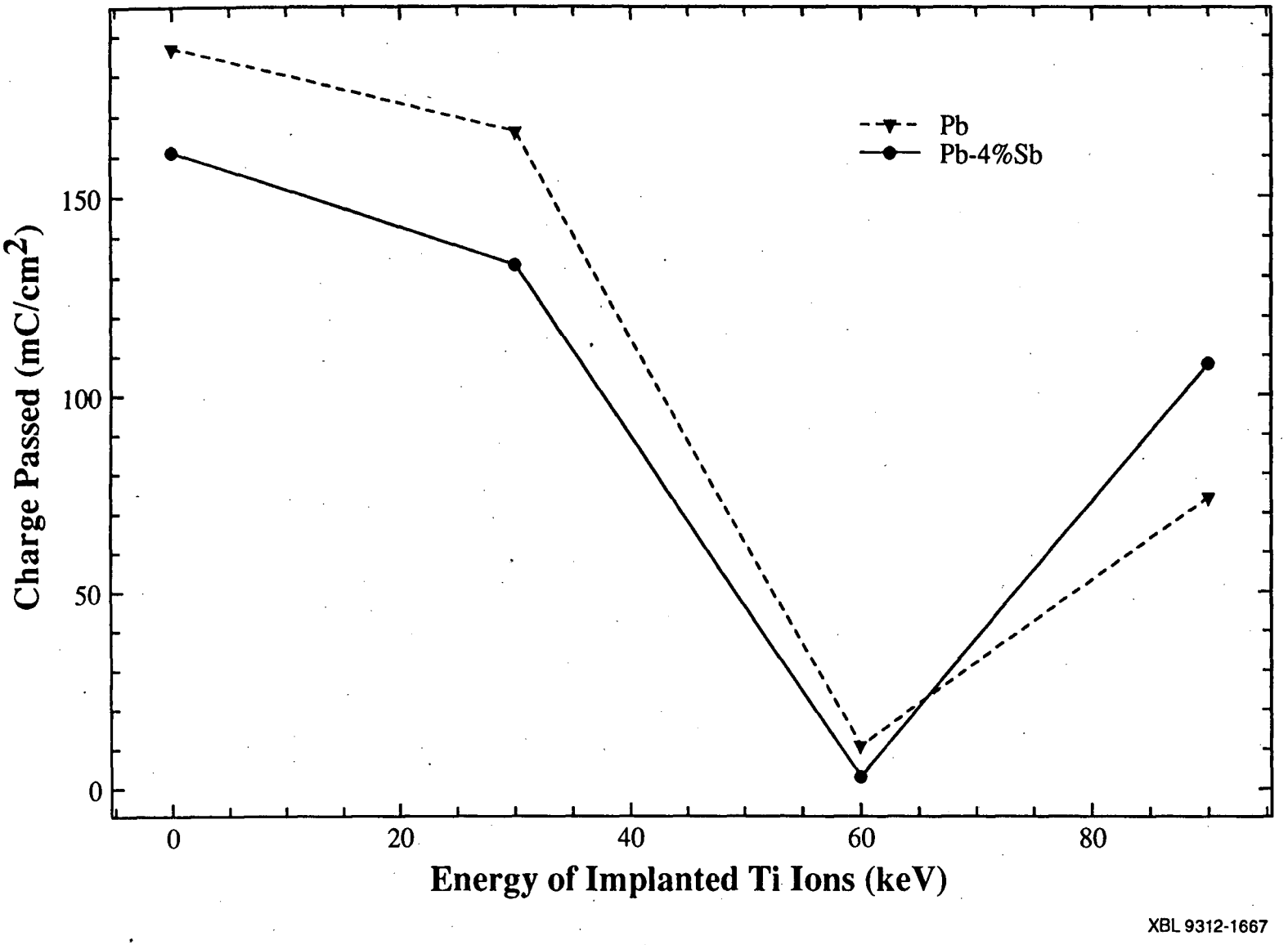
Pb
Pb-4%Sb
Charge Passed (mC/cm^2)
150
100
50
0
0
20
40
60
80
Energy of Implanted Ti Ions (keV)
XBL 9312-1667

Fig. 9

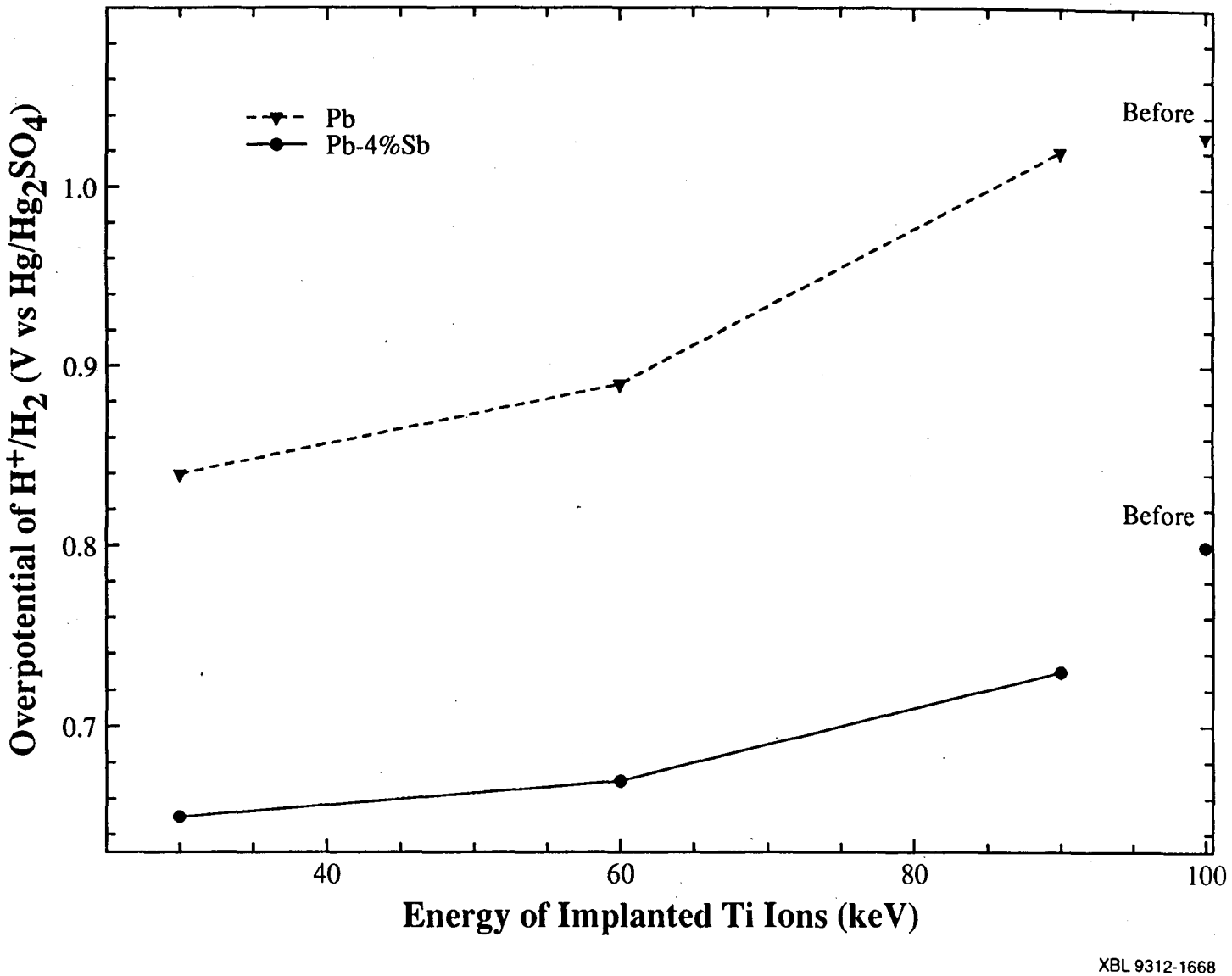
Pb
Pb-4%Sb
Before
Before
Overpotential of H^+/H_2 (V vs Hg/Hg_2SO_4)
1.0
0.9
0.8
0.7
40
60
80
100
Energy of Implanted Ti Ions (keV)
XBL 9312-1668

Fig. 10

LAWRENCE BERKELEY LABORATORY
UNIVERSITY OF CALIFORNIA
TECHNICAL INFORMATION DEPARTMENT
BERKELEY, CALIFORNIA 94720